Ultrasonic synthesized Konjac gum/PEG-silver nanoparticles for colorimetric detection of hydrogen peroxide

SELCAN KARAKUŞ (selcan@istanbul.edu.tr)
ISTANBUL UNIVERSITY-CERRAHPASA https://orcid.org/0000-0002-8368-4609
Nevin Taşaltın
Maltepe Üniversitesi: Maltepe Universitesi
Cihat Taşaltın
TUBITAK MAM: Tubitak Marmara Arastirma Merkezi
Nuray Bekoz Üllen
Istanbul Universitesi-Cerrahpasa

Research Article

Keywords: Nanoparticle, Konjac gum, nanostructure, naked-eye colorimetric, biosensor

Posted Date: February 19th, 2021

DOI: https://doi.org/10.21203/rs.3.rs-212902/v1

Version of Record: A version of this preprint was published at Journal of Inorganic and Organometallic Polymers and Materials on April 2nd, 2021. See the published version at https://doi.org/10.1007/s10904-021-01984-5.

Ultrasonic synthesized Konjac gum/PEG-silver nanoparticles for colorimetric detection of hydrogen peroxide

Selcan Karakuş[1*], Nevin Taşaltın[2, 3,] Cihat Taşaltın [4], Nuray Bekoz Üllen[5]

[1]*İstanbul University-Cerrahpaşa, Dept. of Chemistry, 34320 Istanbul, Turkey*
[2]*Maltepe University, Dept. of Natural Sciences, 34857 Istanbul, Turkey*
[3]*Maltepe University, Dept. of Renewable Energy Tech., 34857 Istanbul, Turkey*
[4]*TÜBİTAK Marmara Researh Center, Materials Institute, Gebze Kocaeli, Turkey*
[5]*Istanbul University-Cerrahpasa, Dept. of Metallurgical and Materials Engineering, 34320 Istanbul, Turkey*

Abstract

Green and low-cost synthesis strategy for ultrasonic preparation of polymer blend matrix based silver nanoparticles (Ag NPs) and the development of rapid and high sensitive detection route have a great attention in biomedical applications. Therefore, in this study, we investigated the hydrogen peroxide detection performance of Konjac gum (KG)/PEG-Ag NPs. The KG/PEG-Ag NPs was synthesized via an ultrasonic process and characterized by different techniques such as ultraviolet–visible spectroscopy (UV–Vis), Fourier-Transform Infrared spectroscopy (FT-IR), Scanning Electron Microscope (SEM) and Energy Dispersive X-ray spectroscopy (EDX). Furthermore, we determined the experimental optimization on the effect of the rheological parameters of nanostructure with the highest correlation constant (R^2: 0.989-0.996), and the intrinsic viscosity (14.71-26.77 dl/g). To provide the miscible polymer blends and homogeneous dispersion of the nanostructure, we compared the rheological parameters with the experimental results. The response time was less than 5 s and the lower limit of detection was 0.071 μM. This novel highly sensitive, rapid, and naked-eye colorimetric biosensor based Ag NPs which are prepared ultrasonic manufacturing approach, opens up a green approach of development facile and rapid detection of hydrogen peroxide in practical biomedical applications.

Keywords: Nanoparticle; Konjac gum; nanostructure; naked-eye colorimetric; biosensor

*Corresponding author. Department of Chemistry, Faculty of Engineering, Istanbul University-Cerrahpasa, 34320 Avcilar, Istanbul, Turkey, Tel.:+90 212 473 7000; fax:+90 212 473 7180, Email address:selcan@istanbul.edu.tr

1. Introduction

Hydrogen peroxide (H_2O_2) is a major biological reactive and the main product of reaction of industrial enzymes such as oxidases, peroxidases, and catalases [1]. It has a role on the cellular damage, apoptosis, pathogen defense mechanism, and mutagenesis in a low concentration in the presence of hydroxyl radicals (OH•) [2-3]. Accordingly, the rapid, low-cost, practical, selective, and sensitive determination of H_2O_2 is very important in different applications such as chemistry, environmental, and biomedical applications [4-5]. In the literature, it was reported that different costly and not portable techniques such as spectrophotometer, chemiluminescence, electrochemical, and electrochemiluminescence were used with complicated procedures for the determination of H_2O_2 [6-9].

In recent years, economical, simple applicable and portable systems such as colorimetric methods have come to the fore in order to eliminate the restrictions on the application [10-14]. Various metal nanoparticles (NPs) such as Ag NPs, gold (Au) NPs, palladium (Pd) NPs, copper (II)-coated Fe_3O_4 NPs, titanium dioxide (TiO_2) NPs, and rhodium NPs have been preferred in the development of H_2O_2 sensors due to the effects of localized surface plasmon resonance energy [15-19]. The localized surface plasmon resonance energy is related to the morphology, composition, size, shape, and dielectric environment of NPs [20]. In this context, Carbone et al. prepared a novel colorimetric sensor based on silver-poly (methyl methacrylate) NPs for the detection of H_2O_2 [21]. Teodoro et al. prepared a colorimetric sensor based on cellulose nanowhiskers and Ag NPs with a low limit of detection of 0.014 μM for the detection of H_2O_2 [22]. Nguyen et al. prepared Ag NPs and graphene quantum dots (AgNPs/GQDs) consisted a colorimetric sensor for H_2O_2 [23]. Huang et al. fabricated a novel dual mode colorimetric and fluorometric sensor with an average diameter of NPs 15.2 nm, which was employed for H_2O_2 detection [24]. In the literature, several green methodologies for use in the synthesis of a biodegradable polymer matrix-based nanostructure have been investigated [25-29]. Chen et. al reported that KG is a polysaccharide form the class of macromolecular carbohydrates and could be used as a reducing and stabilizing agent in the synthesis of Ag NPs [30]. However, there is no study on the ultrasonic synthesized KG/PEG-Ag NPs based colorimetric sensor to be used for detection of H_2O_2.

In this study, the ultrasonic synthesized KG/PEG blend was used as a polymer matrix and the Ag NPs was prepared by a green the ultrasonic method in a liquid at ultrasonic frequencies and characterized via several techniques. Furthermore, we examined the experimental parameters such as the blend of ratios of KG/PEG (wt./wt.) Ag NPs, the sonication time, and the amplitude of the sonication on the viscosities of the ultrasonic synthesized KG/PEG-Ag NPs were investigated to optimize designing conditions. We calculated the intrinsic viscosity of synthesized KG/PEG-Ag NPs. Also, we investigated the effect of H_2O_2 concentration on the colorimetric biosensor.

2. Experimental section

2.1. Materials

KG (Nutricol XP 3464) was obtained from FMC BioPolymer (Philadelphia, USA). Polyethylene glycol (PEG) (Mw= 400kDa) was obtained from Fluka, (Switzerland). Silver nitrate (AgNO3) (ACS reagent, ≥99.0%) was purchased from Merck Company. Omega 3, Testosterone (98%), and progesterone (99%) were obtained from Sigma Chemical Company (St Louis, MO, USA). All chemicals were analytical grade and used as received without further purification.

2.2. Preparation of KG/PEG matrix

KG/PEG-Ag NPs were prepared using a simple and green sonication method. Firstly, 2.5 g of KG was dissolved in 250 mL distilled water. Then, it was kept in the dark for 5 days to gel the solution without stirring. The solution of KG was stirred at 50 °C and filtered using a coarse filter paper and a sterile syringe filter with a 0.45 um pore size, respectively. Thereafter, 12,5 mL of PEG was added into the KG solution and then sonicated for 10 min at 45% amplitude frequency at room temperature.

2.3. Preparation of KG/PEG-Ag NPs

0.84 g of $AgNO_3$ was dissolved in 500 mL distilled water. The Ag solution was slowly added to the KG solution and was stirred at 25 °C for 10 min. 0.1 g of NaOH was dissolved in 250 mL distilled water. The solution of NaOH was slowly added to the KG/PEG blend with

$AgNO_3$ solution until it was stable at pH 8. The solution was sonicated for 10 min at 45% amplitude frequency at 25 °C. Finally, the solution was filtered using a sterile syringe filter with a 0.22 um pore size.

2.4. Characterizations of KG/PEG-Ag NPs

Ultraviolet–visible spectroscopy (UV–Vis) (TG+80 Model), Fourier-Transform Infrared spectroscopy (FT-IR) (Perkin Elmer), scanning electron microscope (SEM) with Energy Dispersive X-ray spectroscopy (EDX) (JEOL JMS-7001F) were used to perform surface characterizations and functional groups of KG/PEG-Ag NPs. We used the viscometer (AND Model) to measure the viscosity of all samples under different experimental conditions. The absorbance values were measured using the UV–Visible spectroscopy with ranging from 300 to 700 nm wavelengths at a resolution of 1 nm in a UV quartz cuvette. We used deionized water as the reference for UV-Vis measurements. The FTIR results were obtained in the frequency range of 4000–400 cm−1 and 8 scans for all samples. SEM images were performed at 20 kV accelerating voltage. All samples were coated with gold using plasma sputtering apparatus before SEM/EDX analysis in a vacuum. The viscosity of all samples was measured using a viscometer (A&D Company Ltd., USA) (type RVT, spindle 18, at 12 rpm and 30Hz with 0.35% reproducibility). The measurement of viscosity of 10 ml volume solutions of all samples were done at constant temperature (in triplicate) in a glass sample cup with a water jacket using a gold sensor plate.

2.5. Rheological analysis of KG/PEG-Ag NPs

We used a simple, easy, and low-cost Dilute Solution Viscometer (DSV) method to characterize the stability of the Ag NPs. We analyzed the rheological parameters of the nanostructure in different experimental conditions and the intrinsic viscosities ([η]), Huggins constant (k), the voluminosity (V_E), and the shape factor (γ) were calculated using Equations 2.1-2.4 (Table 1) [31-33].

Table 1: Equations of rheological parameters and Huggins model

Equations	No
$[\eta] = \frac{\eta_{sp}}{C} = \frac{\eta_{rel} - 1}{C} = \frac{\frac{t}{t_0} - 1}{C}$	(2.1)
${}^{\eta_{sp}}/_{C} = [\eta] + k[\eta]^2 C$ (Huggins model)	(2.2)
$[\eta] = \upsilon V_E$	(2.3)
$\gamma = \frac{\eta_{rel}^{0.5} - 1}{C\,(1.35\eta_{rel}^{0.5} - 0.1)}$	(2.4)

Where C: the concentration of the solution, η_{sp}: the spesific viscosity, η_{rel}: the relative viscosity, t_0: the flow time of the solvent, t: the flow time of the solution, k: Huggins constant, V_E: the voluminosity, and γ: the shape factor.

2.6. Statistical Analysis

All experimental results were performed in triplicate and are given as the mean for each experiment. The analysis of variance (ANOVA) procedure was conducted in SPSS (version 16, Chicago) with a significance level of $P < 0.05$.

3. Results and discussion

3.1. Characterization of KG/PEG-Ag NPs

SEM images of (a) pure KG and (b) KG/PEG-Ag NPs with different magnifications (x10.000 and x40.000) and EDX result of the KG/PEG-Ag NPs (at accelerating voltage of 20 kV) were given in **Fig. 1-2**. According to obtained SEM results, we observed that KG has a regular

fibrous shape and tightly arranged branched structure [34]. Also, the SEM images of Ag NPs were shown that the structure had a spherical shape and small-sized with an average size of 48.8 ± 2 nm [30]. Fig. 3 showed the EDX spectra of the KG/PEG-Ag NPs, in which Ag^{o} were observed at characteristic absorption peaks in the range of 1-2 and 3 keV. The elemental EDX analysis also revealed the presence of C, O, and Ag [35]. Consequently, compared to the SEM images of KG with NPs were observed significant differences. The predicted reason for this is the interaction of Ag NPs with the KG/PEG polymer blend matrix, which had a role as a reducing and stabilizing agent. In addition, the ultrasonic synthesized KG/PEG-Ag NPs exhibited a homogeneous distribution showing the interaction between the polymer blend matrix and the Ag NPs. We assumed that this interaction played a critical role in easily detecting of H_2O_2 with the naked eye in the output signals of a colorimetric biosensor.

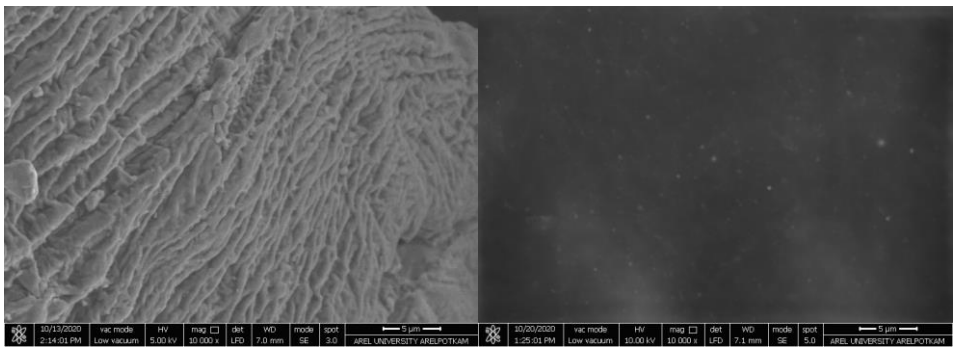

(a) (b)

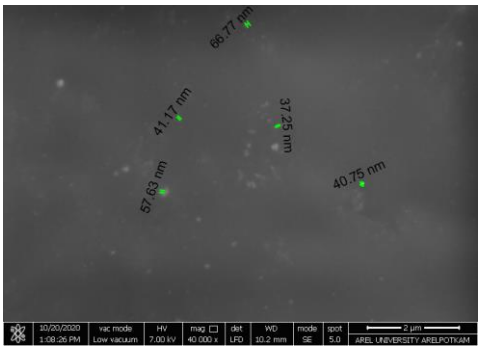

(c)

Figure. 1: SEM images of (a) pure KG and (b) KG/PEG-Ag NPs with different magnifications (x10.000) and (c) (x40.000)

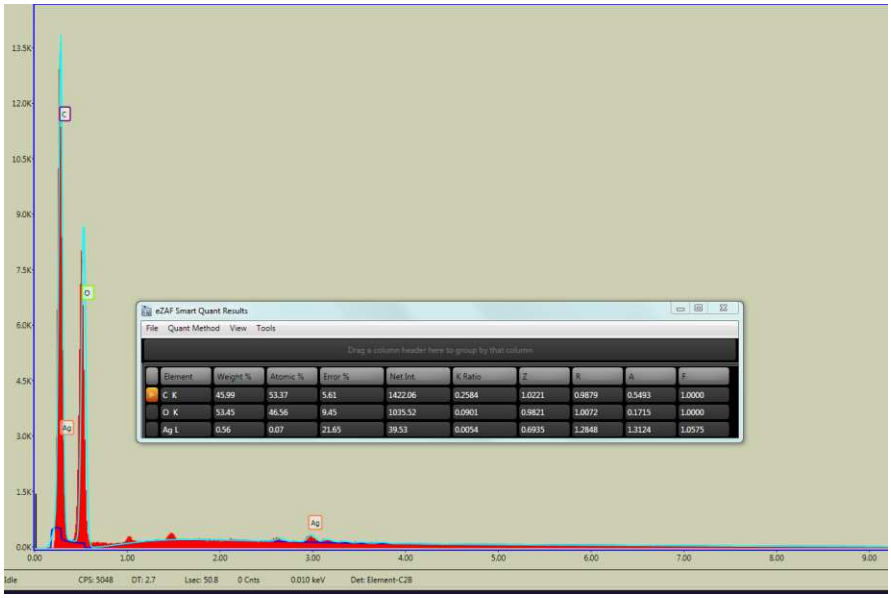

Figure. 2: EDX result of the KG/PEG-Ag NPs

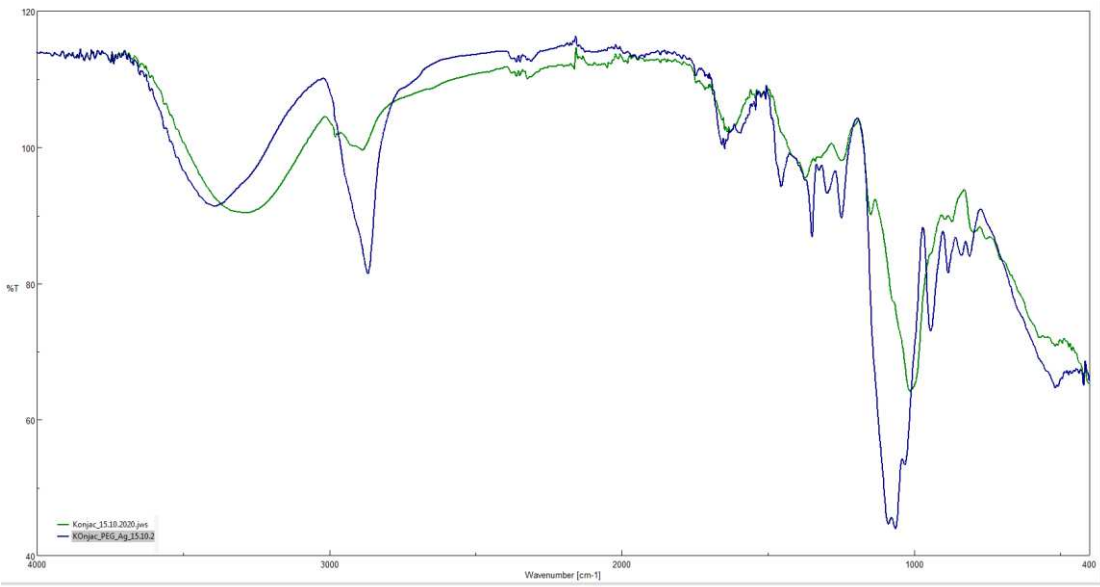

Figure. 3: FTIR analysis of (a) pure KG and (b) KG/PEG-Ag NPs

In **Fig. 3**, FTIR spectra of the pure KG and the ultrasonic synthesized KG/PEG-Ag NPs were given to determine the chemical structure and functional groups of all samples. The characteristic peaks of the pure KG were found at 3276 (-OH stretching), 2890 (C-H stretching), 1628 (OH bending), 1374 (C-H bending), 1250 (C-O bending vibration), and 1014 cm^{-1} (C-O-C stretching) [36-37]. Furthermore, the FTIR of KG/PEG-Ag NPs showed absorption band at 3394 (−OH stretching), 2869 (C–H stretching), 1648 (OH bending), 1456 (-CH_3), 1249 (C-O bending vibration), 1065 (C-O-C symmetrical stretching), and 994 cm^{-1}

(C-O-C symmetrical stretching). However, critical changes in the intensity and position of peak intensity and position for Ag NPs at 3376, 2869 and 1249 cm^{-1} could be attributed to formation of Ag NPs interacting due to –OH and –COOH functional groups have a role on the reduction of Ag^{+} ion to Ag^{0} [38-39]. We assumed that the formation of Ag NPs was due to the electrostatic interaction between the KG/PEG with Ag.

3.2. Viscosity measurement of KG/PEG-Ag NPs

In this study, we prepared KG and PEG polymer blends with Ag NPs using a simple and green sonication method. Also, we investigated to optimize the effects of the experimental conditions such as the blend of ratios of KG/PEG (wt./wt.) (1:1, 1:2, and 1:5) Ag NPs, sonication time (4-10 min) , and amplitude of the sonication (20-45%) on the values of [η] of KG/PEG-Ag NPs (**Fig. 4-7**). Since there are limited studies which focused on the on the role of rheological parameters in the formation, shape, size and miscibility of NPs, this study highlighted the effect of values of the viscosity to design under different experimental conditions [40-42].

The stability, morphology, and uniform particle size distribution of Ag NPs are affected by varying the viscosity as a result of the concentration, temperature, process time, surfactant, and irradiation frequency in the experimental medium [43-45]. One motivating point behind this experimental study is a better understanding of Ag NPs behavior and polymer–polymer interactions in the aqueous solution. For this reason, the interpretation of the experimental viscosity result is a significant issue. In **Fig.4**, we evaluated the viscosity as a function of the ratios of polymer blend KG/PEG (wt./wt.) (1:1, 1:2, and 1:5). The values of [η] of KG/PEG-Ag NPs were determined using the Huggins model. According to rheological experiments, we calculated the values of [η] for KG/PEG-Ag NPs (wt./wt.) (1:1, 1:2, and 1:5) were 14.71, 23.05, and 34.15 dl/g, respectively (**Fig. 4**).

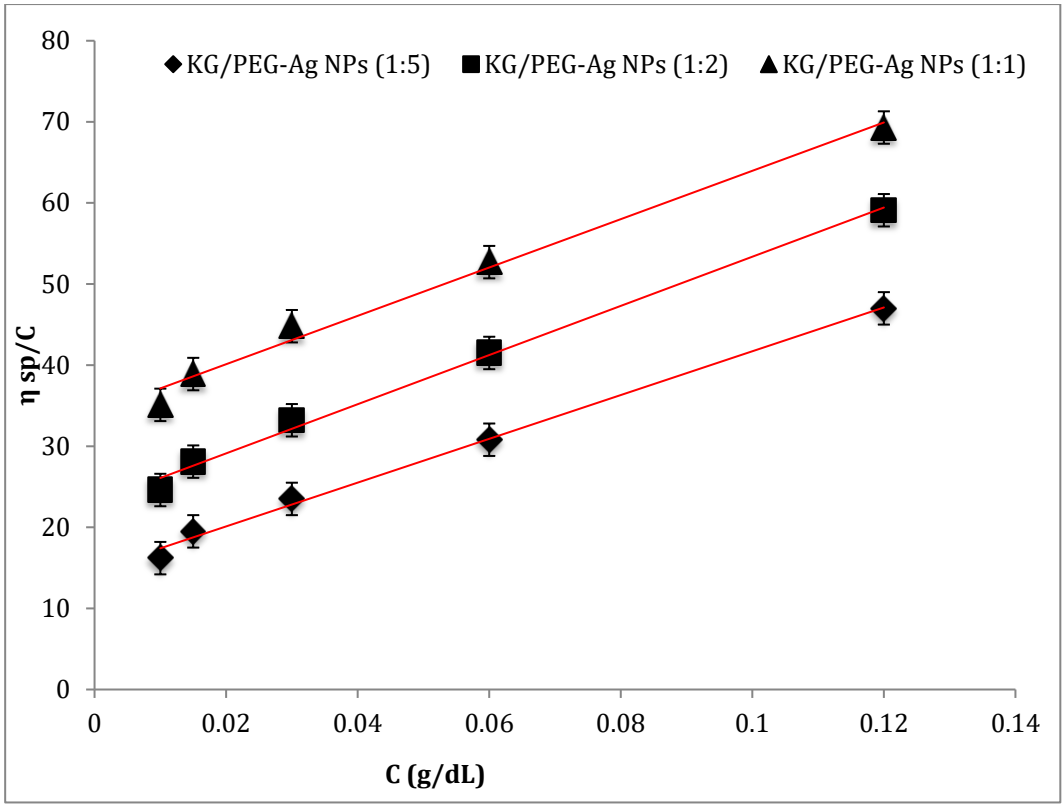

Figure 4: The effect of the blend of ratios of KG/PEG (wt./wt.) (1:1, 1:2, and 1:5) on [η] of the amplitude sonication 45%, sonication time 10 min, and temperature 25°C).

KG/PEG-Ag NPs (wt./wt., 1:1) had the lowest value of [η] with the highest correlation constant (R^2=0.9958) by applying Huggins model. We assumed that these results could be occurred at the high ratio of the PEG as a plasticizer interacting the hydroxyl end groups of PEG with the acetyl groups in the KG due to the intermolecular hydrogen bonding [46-47].

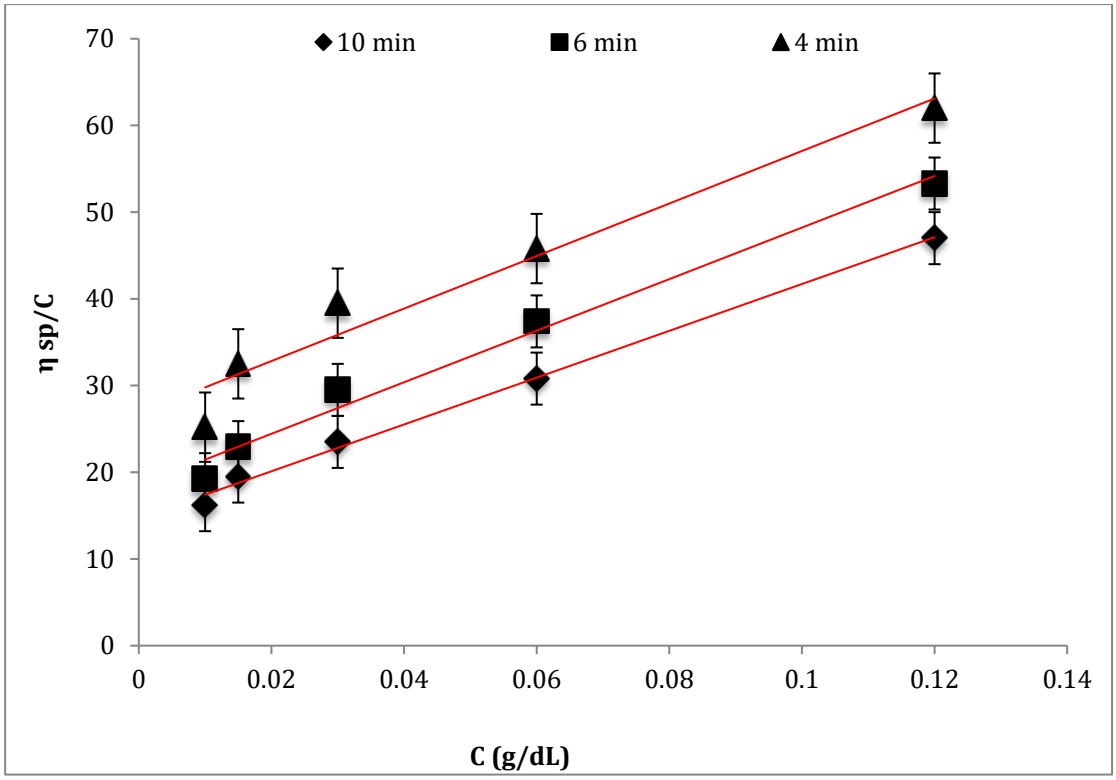

Figure 5: The effect of the sonication time (4-10 min) on [η] of KG/PEG-Ag NPs (ratio 1:5, the amplitude sonication 45%, and temperature 25°C)

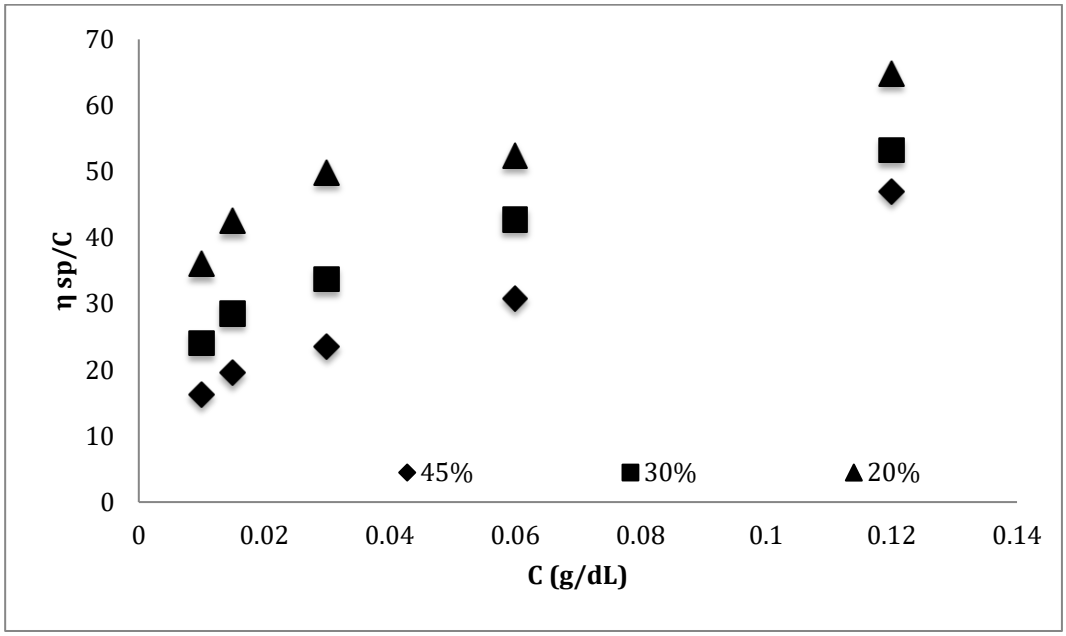

Figure 6: The effect of the amplitude of the sonication (20-45%) on [η] of KG/PEG-Ag NPs (the ratio of KG/PEG 1:5, sonication time 10 min, and temperature 25°C)

The values of [η] at different sonication times (4-10 min) were calculated for KG/PEG-Ag NPs (1:5) at the amplitude sonication 45%, and temperature 25ºC. These viscosity results were given in **Fig. 5**. The values of [η] of the sonochemical synthesized KG/PEG-Ag NPs (1:5) at different sonication times (4-10 min) were calculated and these results were 14.71 dl/g for 4 min, 18.48 dl/g for 6 min, and 26.77 dl/g for 10 min. We found the minimum viscosity was 14.71 dl/g for at amplitude 45% (**Fig. 6)**. When the experimental data were compared, we observed that the sonication time and the values of amplitude were important parameters in determining the viscosity at the optimum conditions, from the low [η] value.

Table. 2: The voluminosity and shape factors for the KG/PEG-Ag NPs (1: 5)

KG/PEG-Ag NPs	[η]	ϒ	Shape
1:1	14.71±0.12	0.26 (less than 2.5)	Spherical
1:2	23.05±0.18	0.38 (less than 2.5)	
1:5	34.15±0.22	0.55 (less than 2.5)	

*Values are means ± standard deviation (SD) for triplicate determination

By applying Eqs.2.3-2.4, V_E and [η] via shape factor (υ) were calculated. The V_E was calculated through intercept of plotting γ versus C. As it is known, υ is a parameter to show the shape of the structure as υ> 2.5 it indicates ellipsoidal and υ <2.5 it indicates spherical shape. Our results proved that the nanostructures had a spherical shape since the values of υ of KG / PEG-Ag NPs were less than 2.5 [48].

3.3. Colorimetric measurement of KG/PEG-Ag NPs for the detection of H_2O_2

For determination of selectivity of the novel colorimetric biosensor, we compared the color changes of the sample in the presence of Omega 3, testosterone, progesterone, and H_2O_2 was taken photographed using a Nikon D5100 + 18-55mm lens digital SLR camera (**Fig. 7**). All of the colorimetric experimental runs were carried out in the presence of phosphate buffered saline (pH 7.4) (PBS) and results were compared for H_2O_2, Omega 3, testosterone, and progesterone by varying the concentrations of sample 1 to 100 μM. For colorimetric measurements, at first, the different concentrations of 100 μL of H_2O_2solution were added to $10mL^{-1}$ of Ag NPs. We observed the color changing of the sample yellow to transparent by naked eye in 5 seconds (response time).

Also, we measured the absorbance of the final solution at 462 nm using an UV–Vis spectrophotometer. It was monitored that the novel colorimetric biosensor selectively detected H_2O_2, although other samples in the presence of Omega 3, testosterone, and progesterone had a phase separation, turbidity and long-term detection.

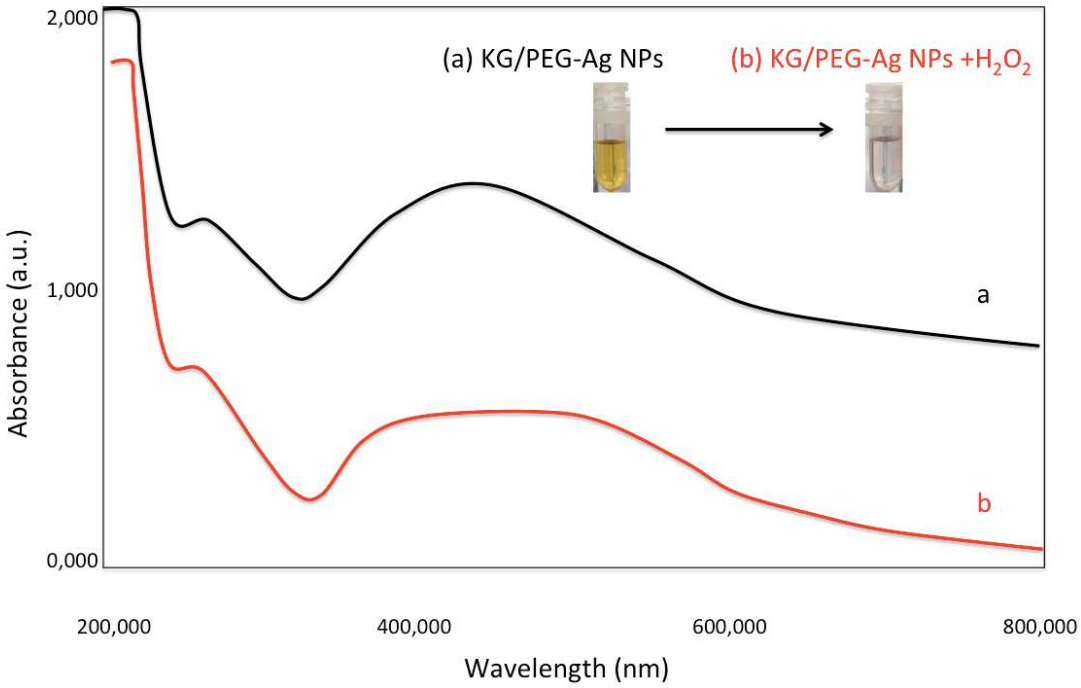

(a)

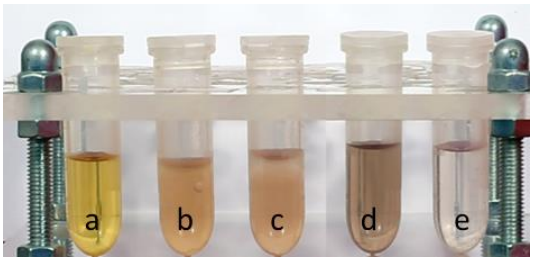

(b)

Figure 7: (A) UV-vis absorption spectra of KG/PEG-Ag NPs and KG/PEG-Ag NPs + H_2O_2, (B) Photographs of the selective colorimetric measurements of KG/PEG-Ag NPs (1:5) with different analytes such as (a) KG/PEG-Ag NPs in the absence of analyte, (b) in the presence of Omega 3, (c) testosterone, (d) progesterone, and (e) hydrogen peroxide

The colorimetric measurements were performed to determine the sensitivity of KG/PEG-Ag NPs by varying the concentrations of H_2O_2 1 to 100 µM. The results were given in **Fig. 8**. As

shown, the highest absorption intensity (ΔA) variation (Eq 3.1) was found for H_2O_2 at 100 μM.

$$\Delta A = A_0 - A_t \quad (3.1)$$

Where; Ao: the absorbance of KG/PEG-Ag NPs and A_t: the absorbance of KG/PEG-Ag NPs + H_2O_2 at t time.

We found the determination of the detection limit (D.L.) (Eq. 3.2) and it was based on the value of SD of the response (σ) and the slope (S) of the plot of KG/PEG-Ag NPs at 462 nm.

$$D.L. = 3\,\sigma/S \quad (3.2)$$

The KG/PEG-Ag NPs also had a lower limit of detection (0.071 μM) and the response time was ~5 s.

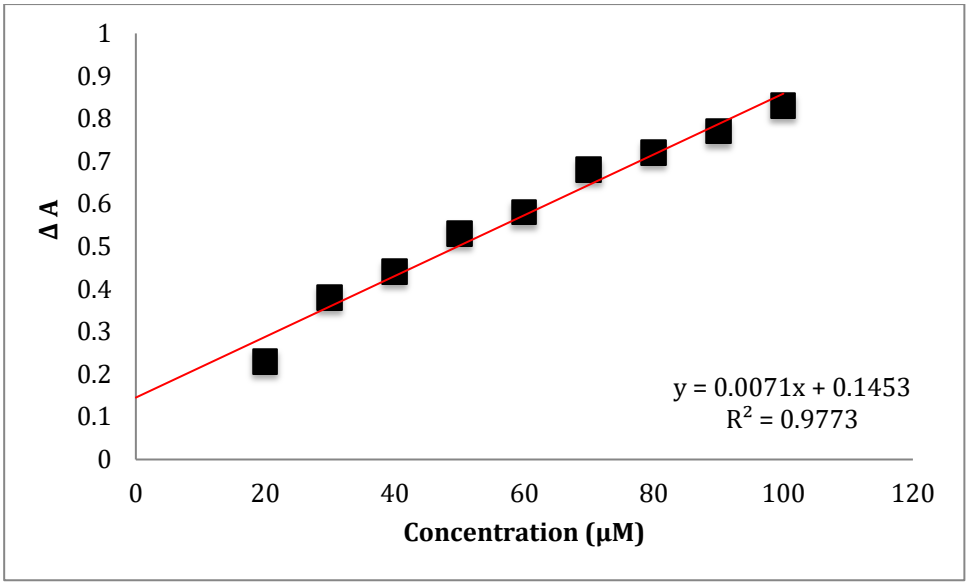

(a)

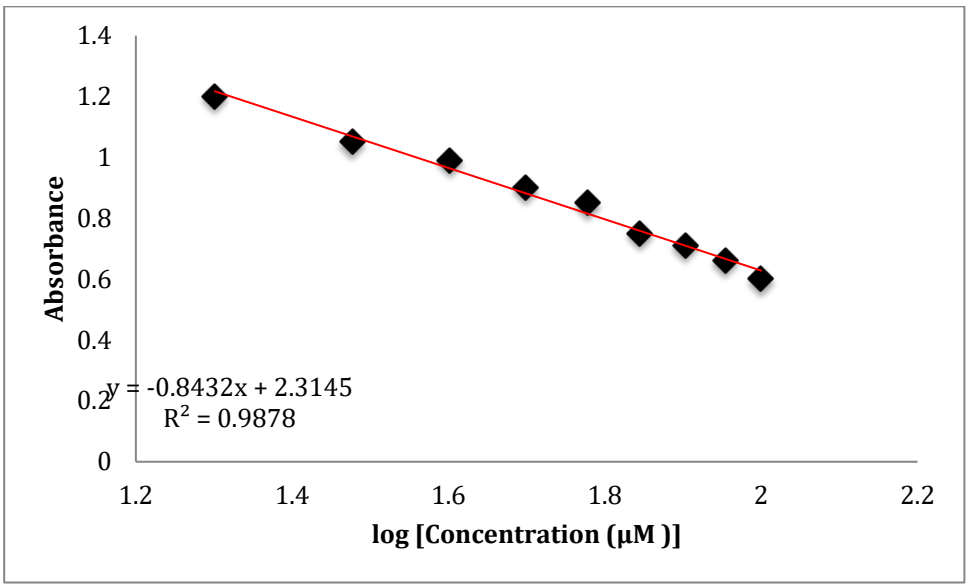

(b)

Figure 8: The linear calibration plots of (a) the absorption intensity (ΔA), and (b) the absorbance of the KG/PEG-Ag NPs by varying the concentrations of H_2O_2 (1 -100 µM)

This study aimed to investigate the rapid response of a newly developed KG/PEG-Ag NPs based colorimetric biosensor having a potential selectivity for the detection of H_2O_2 dependent degradation of Ag NPs in biomedical applications. According from our results, the estimated detection mechanism was described in Eqs. 3.3.

$H_2O_2 + 2H^+ + KG/PEG\text{-}Ag^o \leftrightarrow KG/PEG\text{-}2Ag^+ + 2\ H_2O$ (3.3)

The transformation of the yellow KG/PEG-Ag NPs to a transparent color in the presence of H_2O_2 analyte enabled it to be perceived with the naked eye in the detection of H_2O_2. This possible mechanism was due to the oxidation of Ag^0 to Ag^+ ions with the electrocatalytic ability of KG/PEG-Ag NPs [21]. These results of the novel colorimetric biosensor were appreciable from the comparison with results of previous studies in the literature (Table 3).

Table. 3: The comparison of analytical performance of the various electrodes for the detection of H_2O_2.

Sample	Method	Linear Range	References
Cellulose nanowhiskers and Ag NPs	Ultrasonic	0.01 μM−30 μM 60–600 μM	[22]
Ag and Au NPs	Chemical reduction	1.25 μM to 1250 μM	[49]
Wheat straw extracted lignin in Ag NPs	Chemical reduction	1-100 μM	[50]
Acacia lignin stabilized Ag NPs	Chemical reduction	5–500 μg/ml	[51]
Silver chloride NPs (AgCl-NPs)	Solution	1–120 μM	[20]
KG/PEG-Ag NPs	Ultrasonic	1-100 μM	This study

3.3. Stability of KG/PEG-Ag NPs

In this study, the stability of KG/PEG-Ag NPs solution (5.0 mL) was evaluated under the ultraviolet light (365 nm) for 1 h. We measured the amount of remaining sample every 10 min. In order to evaluate the effect of the ultraviolet factor on KG/PEG-Ag NPs (1:5), the stability of KG/PEG-Ag NPs was examined by their intrinsic viscosity value. As a result, it was seen that the nanostructure had a stable structure in **Fig. 9.** Also, it was proved that the viscosity value was slightly affected by ultraviolet light. It was found that there was an 8.51% change of [η] after 60 minutes. There are no systematic studies on the stability of Ag NPs in the literature to determine the change in [η] of the nanostructure under the ultraviolet irradiation.

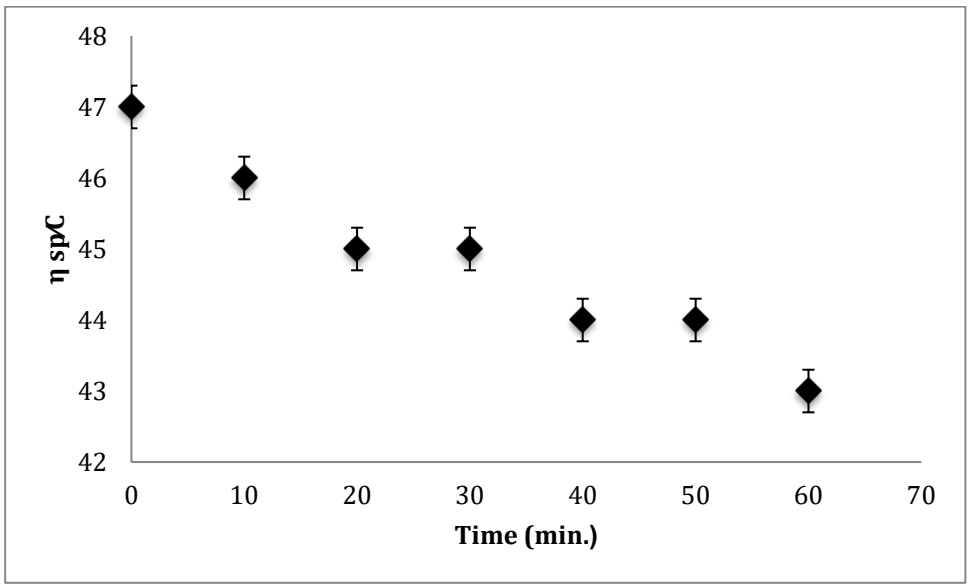

Figure 9: The effect of the ultraviolet factor on KG/PEG-Ag NPs (1:5) on [η]

4. CONCLUSION

This study demonstrated that the highly sensitive and naked eye colorimetric biosensor for the detection of H_2O_2 based on spherical KG/PEG- Ag NPs. Furthermore, the experimental optimization on the effect of the rheological parameters of nanostructure with the highest correlation constant (R^2: 0.989-0.996), and the intrinsic viscosity (14.71-26.77 dl/g) was calculated. KG/PEG- Ag NPs (1:5) showed the higher stability and selectivity for hydrogen peroxide in PBS. We observed the color changing of the sample yellow to transparent by naked eye in 5 seconds (response time) with 0.071 μM the lower limit of detection. This novel

highly sensitive, rapid, and naked-eye colorimetric biosensor based on KG/PEG- Ag NPs has a potential sensor facile and rapid detection of hydrogen peroxide in practical applications.

Acknowledgment:

Declaration of Competing Interest

The authors declare that they have no conflict of interests.

References:

[1] C. Richter-Landsberg, U. Vollgraf, Mode of cell injury and death after hydrogen peroxide exposure in cultured oligodendroglia cells. Experimental cell research. **244**(1), 218-229 (1998) https://doi.org/10.1006/excr.1998.4188.

[2] C. Emily, A.J. Friedman, Hydrogen peroxide and cutaneous biology: Translational applications, benefits, and risks. Journal of the American Academy of Dermatology. **81**(6), 1379-1386 (2019) https://doi.org/10.1016/j.jaad.2019.05.030.

[3] B.J. Juven, M.D. Pierson, Antibacterial effects of hydrogen peroxide and methods for its detection and quantitation. Journal of Food Protection. **59**(11), 1233-1241 (1996) https://doi.org/10.4315/0362-028X-59.11.1233.

[4] V. Gautam, K.P. Singh, V.L. Yadav, Polyaniline/multiwall carbon nanotubes/starch nanocomposite material and hemoglobin modified carbon paste electrode for hydrogen peroxide and glucose biosensing. International journal of biological macromolecules. **111**, 1124-1132 (2018) https://doi.org/10.1016/j.ijbiomac.2018.01.094.

[5] A. Ngamaroonchote, Y. Sanguansap, T. Wutikhun, K. Karn-Orachi, Highly branched gold–copper nanostructures for non-enzymatic specific detection of glucose and hydrogen peroxide. Microchim Acta. 187, 2-12 (2020) https://doi.org/10.1007/s00604-020-04542-x.

[6] U. Sivasankaran, T.C. Jos & K.G. Kumar, Selective recognition of creatinine–Development of a colorimetric sensor. Analytical biochemistry. **544**, 1-6 (2018) https://doi.org/10.1016/j.ab.2017.12.017.

[7] S. Bocanegra-Rodríguez, N. Jornet-Martínez, C. Molins-Legua, P. Campíns-Falcó, New Reusable Solid Biosensor with Covalent Immobilization of the Horseradish Peroxidase Enzyme: In Situ Liberation Studies of Hydrogen Peroxide by Portable Chemiluminescent Determination, ACS omega. **5**(5), 2419-2427 (2020) https://doi.org/10.1021/acsomega.9b03958.

[8] I.W. Cho, S.U. Son, M. Yang, J. Choi, Preparation of microporous MoS2@ carbon nanospheres for the electrochemical detection of hydrogen peroxide. Journal of Electroanalytical Chemistry. **876**, 114739 (2020) https://doi.org/10.1016/j.jelechem.2020.114739.

[9] L. Wang, X.H. Shi, Y.F. Zhang, A.A. Liu, S.L. Liu, Z.G. Wang, D.W. Pang, CdZnSeS quantum dots condensed with ordered mesoporous carbon for high-sensitive electrochemiluminescence detection of hydrogen peroxide in live cells. Electrochimica Acta. **362**, 137107 (2020). https://doi.org/10.1016/j.electacta.2020.137107.

[10] Y. Leng, J. He, B. Li, X. Xing, Y. Guo, L. Ye, & Z. Lu, The effects of colorimetric detection of heavy metal ions based on Au nanoparticles (NPs): size and shape—a case of Co 2+. Applied Physics A, 123(9), 1-9 (2017). https://doi.org/10.1007/s00339-017-1225-6

[11] A. Suea-Ngam, L.T. Deck, P.D. Howes, A.J. DeMello, An ultrasensitive non-noble metal colorimetric assay using starch-iodide complexation for Ochratoxin A detection. Analytica Chimica Acta. **1135**, 29-37 (2020) https://doi.org/10.1016/j.aca.2020.08.028.

[12] C. Liu, Y. Miao, X. Zhang, S. Zhang, X. Zhao, Colorimetric determination of cysteine by a paper-based assay system using aspartic acid modified gold nanoparticles. Microchimica Acta. **187**, 362 (2020) https://doi.org/10.1007/s00604-020-04333-4.

[13] Z. Du, C. Wei, Using G-Rich Sequence to Enhance the Peroxidase-Mimicking Activity of DNA-Cu/Ag Nanoclusters for Rapid Colorimetric Detection of Hydrogen Peroxide and Glucose. ChemistrySelect. **5**(17), 5166-5171 (2020)https://doi.org/10.1002/slct.202000956.

[14] L. Zhang, X. Hai , C. Xia, X.W. Chen, J.H. Wang, Growth of CuO nanoneedles on graphene quantum dots as peroxidase mimics for sensitive colorimetric detection of hydrogen peroxide and glucose. Sensors and Actuators B: Chemical. **248**, 374-384 (2017) https://doi.org/10.1016/j.snb.2017.04.011.

[15] P.J. Rivero, E. Ibañez, J. Goicoechea, A. Urrutia, I.R. Matias, F.J. Arregui, A self-referenced optical colorimetric sensor based on silver and gold nanoparticles for quantitative determination of hydrogen peroxide. Sensors and Actuators B: Chemical. **251**, 624-631 (2017) https://doi.org/10.1016/j.snb.2017.05.110.

[16] Z. Yang, Z. Zhang, Y. Jiang, M. Chi, G. Nie, X. Lu, C. Wang, Palladium nanoparticles modified electrospun CoFe2O4 nanotubes with enhanced peroxidase-like activity for

colorimetric detection of hydrogen peroxide. RSC advances. **6**(40), 33636-33642 (2016) https://doi.org/10.1039/C6RA01527A.

[17] H. Liu, L. Zhu, H. Ma, J. Wen, H. Xu, Y. Qiu, L. Zhang, L. Li, C. Gu, Copper (II)-coated Fe_3O_4 nanoparticles as an efficient enzyme mimic for colorimetric detection of hydrogen peroxide. Microchimica Acta. **186**(8), 518 (2019) https://doi.org/10.1007/s00604-019-3599-y.

[18] B. Gökdere, A. Üzer, S. Durmazel, E. Erçağ, R. Apak, Titanium dioxide nanoparticles–based colorimetric sensors for determination of hydrogen peroxide and triacetone triperoxide (TATP). Talanta. **202**, 402-410 (2019) https://doi.org/10.1016/j.talanta.2019.04.071.

[19] J. N'Diaye, S. Poorahong, O. Hmam, R. Izquierdo, M. Siaj, Facile synthesis rhodium nanoparticles decorated single layer graphene as an enhancement hydrogen peroxide sensor. Journal of Electroanalytical Chemistry. **789**, 85-91 (2017) https://doi.org/10.1016/j.jelechem.2017.01.061.

[20] M. Farrokhnia S. Karimi, S. Momeni, S. Khalililaghab, Colorimetric sensor assay for detection of hydrogen peroxide using green synthesis of silver chloride nanoparticles: Experimental and theoretical evidence. Sensors and Actuators B: Chemical. **246**, 979-987 (2017) https://doi.org/10.1016/j.snb.2017.02.066.

[21] G.G. Carbone, A. Serra, A. Buccolieri, & D. Manno, A silver nanoparticle-poly (methyl methacrylate) based colorimetric sensor for the detection of hydrogen peroxide. Heliyon. **5**(11), 02887 (2019). https://doi.org/10.1016/j.heliyon.2019.e02887.

[22] K.B. Teodoro, F.L. Migliorini, W.A. Christinelli, & D.S. Correa, Detection of hydrogen peroxide (H2O2) using a colorimetric sensor based on cellulose nanowhiskers and silver nanoparticles. Carbohydrate polymers. **212**, 235-241 (2019) https://doi.org/10.1016/j.carbpol.2019.02.053.

[23] N.D. Nguyen, T. Van Nguyen, A.D. Chu, H.V. Tran, L.T. Tran, & C.D. Huynh, A label-free colorimetric sensor based on silver nanoparticles directed to hydrogen peroxide and glucose. Arabian Journal of Chemistry. **11**(7), 1134-1143 (2018) https://doi.org/10.1016/j.arabjc.2017.12.035.

[24] Huang, H. X. Zhou, Y. Huang, H. Jiang, N. Yang, S.A. Shahzad, L. Meng, C. Yu, Silver nanoparticles decorated and tetraphenylethene probe doped silica nanoparticles: A colorimetric and fluorometric sensor for sensitive and selective detection and intracellular imaging of hydrogen peroxide. Biosensors and Bioelectronics. **121**, 236-242 (2018) https://doi.org/10.1016/j.bios.2018.09.023.

[25] K. Roy, S. Lahiri, A green method for synthesis of radioactive gold nanoparticles. Green Chemistry. **8**(12), 1063-1066 (2006) https://doi.org/10.1039/B605625C.

[26] S.K. Shukla, S.K. Shukla, P.P. Govender, & N.G. Giri, Biodegradable polymeric nanostructures in therapeutic applications: opportunities and challenges. RSC advances. **6**(97), 94325-94351 (2016) DOI: 10.1039/C6RA15764E

[27]A. K. Taha, M. Amir, A. D. Korkmaz, M. A. Al-Messiere, A. Baykal, S. Karakuş, A. Kilislioglu, Development of novel nano-ZnO enhanced polymeric membranes for water purification, Journal of Inorganic and Organometallic Polymers and Materials. **29**(3), 979-988 (2019). https://doi.org/10.1007/s10904-018-0988-3.

[28] S. Ghayempour, M. Montazer, Ultrasound irradiation based in-situ synthesis of star-like Tragacanth gum/zinc oxide nanoparticles on cotton fabric, Ultrasonics sonochemistry. **34**, 458-465 (2017).

[29] J. Balachandramohan, T. Sivasankar, M. Sivakumar, Facile sonochemical synthesis of Ag2O-guar gum nanocomposite as a visible light photocatalyst for the organic transformation reactions. Journal of hazardous materials. **385**, 121621 (2020). https://doi.org/10.1016/j.jhazmat.2019.121621.

[30] J. Chen, Y. Liu, Y. Xiong, D. Wei, J. Peng, S. Mahmud, H. Liu, Konjac glucomannan reduced-stabilized silver nanoparticles for mono-azo and di-azo contained wastewater treatment. Inorganica Chimica Acta. **515**, 120058 (2021). https://doi.org/10.1016/j.ica.2020.120058.

[31] S. Karakuş, Preparation and rheological characterization of Chitosan-Gelatine@ ZnO-Si nanoparticles, International journal of biological macromolecules. **137**, 821-828 (2019). https://doi.org/10.1016/j.ijbiomac.2019.06.231.

[32] S. Karakuş, M. Ilgar, I. M. Kahyaoglu, A. Kilislioglu, Influence of ultrasound irradiation on the intrinsic viscosity of guar gum–PEG/rosin glycerol ester nanoparticles, International journal of biological macromolecules. **141**, 1118-1127 (2019). https://doi.org/10.1016/j.ijbiomac.2019.08.254.

[33] X. Ma, M. Pawlik, Intrinsic viscosities and Huggins constants of guar gum in alkali metal chloride solutions, Carbohydrate Polymers. **70**(1), 15-24 (2007). https://doi.org/10.1016/j.carbpol.2007.02.024.

[34] L. X. Wang, A. R. Lee, Y. Yuan, X. M. Wang, T. J. Lu, and FTIR, Raman and SEM characterizations of Konjac Glucomannan-KCl electrogels. Food Chemistry. **331**, 127289 (2020). https://doi.org/10.1016/j.foodchem.2020.127289.

[35] N. Hashim, M. Paramasivam, J.S. Tan, D. Kernain, M.H. Hussin, N. Brosse, F. Gambier, P.B. Raja, Green mode synthesis of silver nanoparticles using Vitis vinifera's tannin and screening its antimicrobial activity/apoptotic potential versus cancer cells. Materials Today Communications. **25**, 101511 (2020). https://doi.org/10.1016/j.mtcomm.2020.101511.

[36] D.F. Da Silva, C.Y.L. Ogawa, F. Sato, A.M. Neto, F.H. Larsen, P.T. Matumoto-Pintro, Chemical and physical characterization of Konjac glucomannan-based powders by FTIR and 13C MAS NMR, Powder Technology. **361**, 610-616 (2020). https://doi.org/10.1016/j.powtec.2019.11.071.

[37] J. Wu, X. Deng, X. Lin, Swelling characteristics of konjac glucomannan superabsobent synthesized by radiation-induced graft copolymerization, Radiation Physics and Chemistry. **83**, 90-97 (2013). https://doi.org/10.1016/j.radphyschem.2012.09.026.

[38] K. Ponsanti, B. Tangnorawich, N. Ngernyuang, C. Pechyen, A flower shape-green synthesis and characterization of silver nanoparticles (AgNPs) with different starch as a reducing agent, Journal of Materials Research and Technology. **9**(5), 11003-11012 (2020). https://doi.org/10.1016/j.jmrt.2020.07.077.

[39] S. Pugazhendhi, Synthesis of ipomoea staphylina plant extract mediated silver nanoparticles, Materials Today: Proceedings. (2020). https://doi.org/10.1016/j.matpr.2020.08.287.

[40] X. Hu, D. Yin, X. Chen, G. Xiang, Experimental investigation and mechanism analysis: Effect of nanoparticle size on viscosity of nanofluids. Journal of Molecular Liquids. **314**, 113604 (2020). https://doi.org/10.1016/j.molliq.2020.113604.

[41] A.L. Elrefai, T. Yoshida, K. Enpuku, Viscosity dependent amplitude and phase of harmonic signals of magnetic nanoparticles. Journal of Magnetism and Magnetic Materials. **507**, 166809 (2020). https://doi.org/10.1016/j.jmmm.2020.166809.

[42] J. Sunil, S.N. Alex, A.A. Pravin, M.D. Pooja, R. Ginil, Thermal properties of aqueous silver nanoparticle dispersion, Materials Today: Proceedings. (2020). https://doi.org/10.1016/j.matpr.2020.04.069.

[43] J. Zhou, M. Hu, D. Jing, The synergistic effect between surfactant and nanoparticle on the viscosity of water-based fluids, Chemical Physics Letters. **727**, 1-5 (2019). https://doi.org/10.1016/j.cplett.2019.04.052.

[44] X. Shen, X. Sun, J. Liu, J. Hang, L. Jin, L. Shi, A facile strategy to achieve monodispersity and stability of pigment TiO_2 particles in low viscosity systems, Journal of Colloid and Interface Science. **581**, 586-594 (2021). https://doi.org/10.1016/j.jcis.2020.07.132.

[45] H. Attari, F. Derakhshanfard, M.H.K. Darvanjooghi, Effect of temperature and mass fraction on viscosity of crude oil-based nanofluids containing oxide nanoparticles, International Communications in Heat and Mass Transfer. **82**, 103-113 (2017). https://doi.org/10.1016/j.icheatmasstransfer.2017.02.007.

[46] Y. Jiang, J. Huang, X. Wu, Y. Ren, Z. Li, J. Ren, Controlled release of silver ions from AgNPs using a hydrogel based on konjac glucomannan and chitosan for infected wounds, International Journal of Biological Macromolecules. **149**, 148-157 (2020).

[47] M. Sheikholeslam, M.E.E. Wright, M.G. Jeschke, S. Amini-Nik, Biomaterials for skin substitutes. Advanced healthcare materials. **7**(5), 17008997 (2018). https://doi.org/10.1002/adhm.201700897.

[48] A. Heydari, S.M.A. Razavi, M. Irani, Effect of temperature and selected sugars on dilute solution properties of two hairless canary seed starches compared with wheat starch, International journal of biological macromolecules. **108**, 1207-1218 (2018). https://doi.org/10.1016/j.ijbiomac.2017.11.026.

[49] P.J. Rivero, E. Ibañez, J. Goicoechea, A. Urrutia, I.R. Matias, F.J. Arregui, A self-referenced optical colorimetric sensor based on silver and gold nanoparticles for quantitative determination of hydrogen peroxide, Sensors and Actuators B: Chemical. **251**, 624-631 (2017). https://doi.org/10.1016/j.snb.2017.05.110.

[50] R.G. Saratale, G.D. Saratale, G. Ghodake, S.K. Cho, A. Kadam, G. Kumar, B.H. Jeon, A. Bhatnagar, H.S. Shin, Wheat straw extracted lignin in silver nanoparticles synthesis: Expanding its prophecy towards antineoplastic potency and hydrogen peroxide sensing ability, International journal of biological macromolecules. **128**, 391-400 (2019). https://doi.org/10.1016/j.ijbiomac.2019.01.120.

[51] K.R. Aadil, A. Barapatre, A.S. Meena, H. Jha, Hydrogen peroxide sensing and cytotoxicity activity of Acacia lignin stabilized silver nanoparticles, International journal of biological macromolecules. **82**, 639-47 (2016). https://doi.org/10.1016/j.ijbiomac.2015.09.072.

Figures

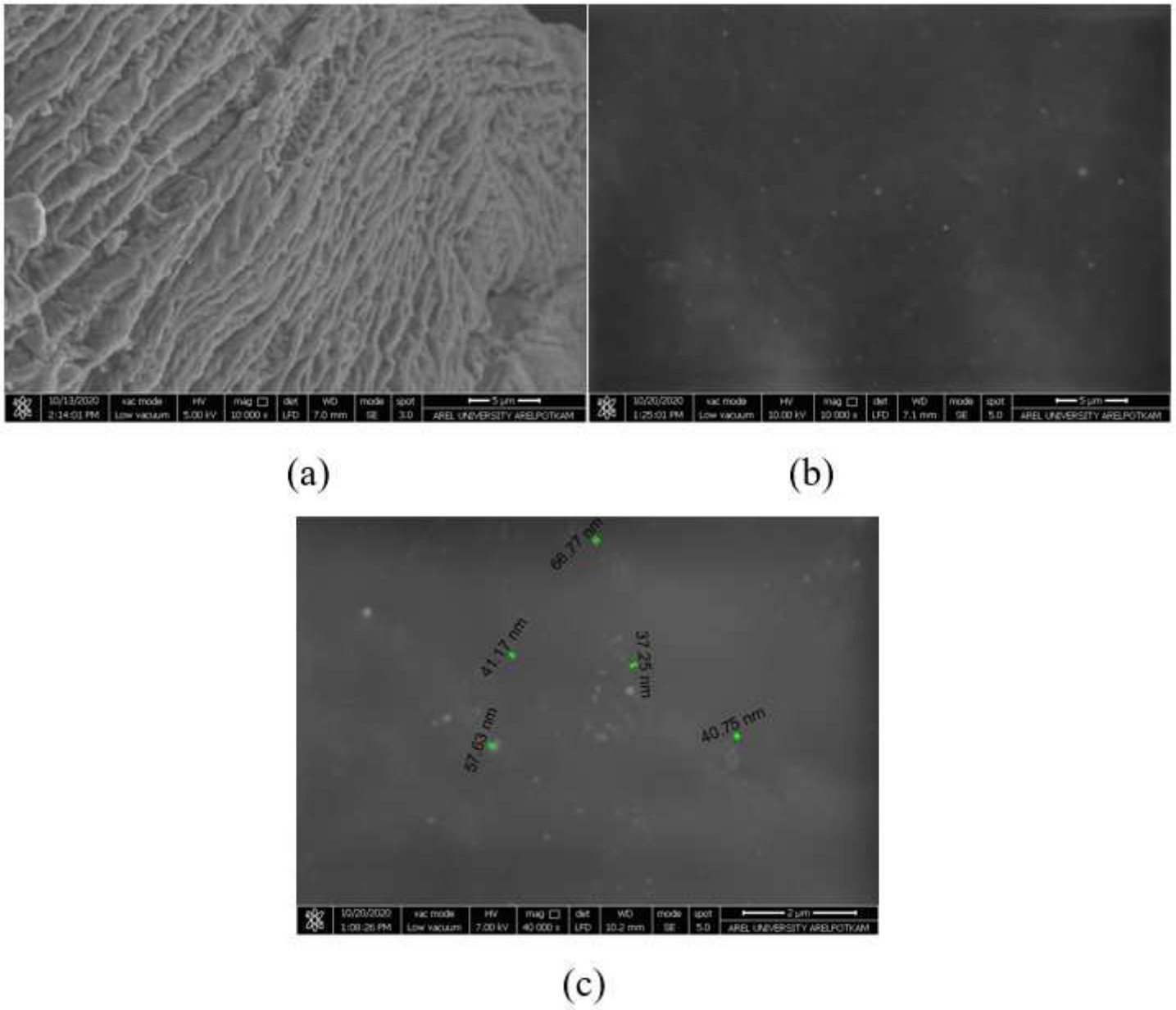

Figure 1

SEM images of (a) pure KG and (b) KG/PEG-Ag NPs with different magnifications (x10.000) and (c) (x40.000)

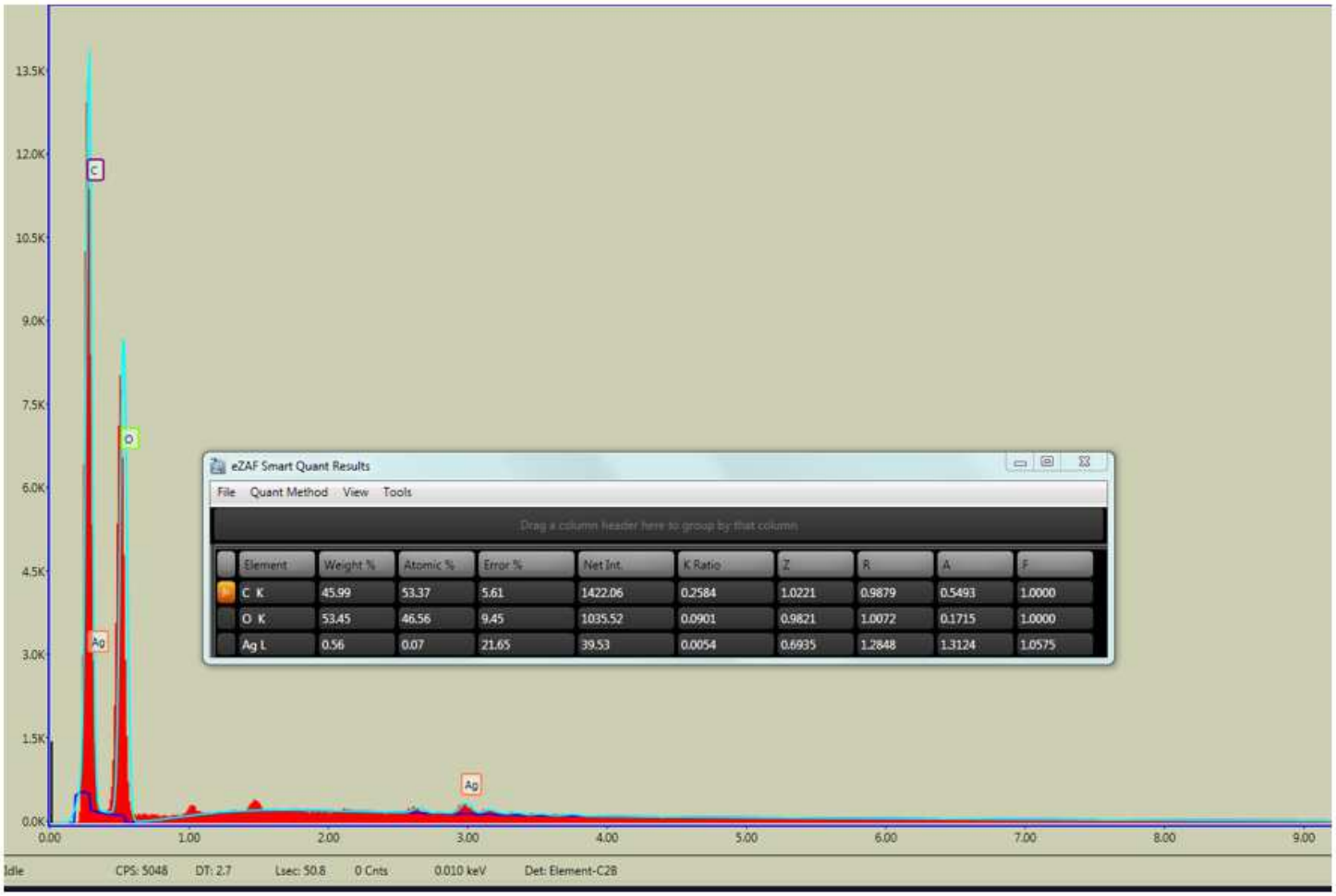

Figure 2

EDX result of the KG/PEG-Ag NPs

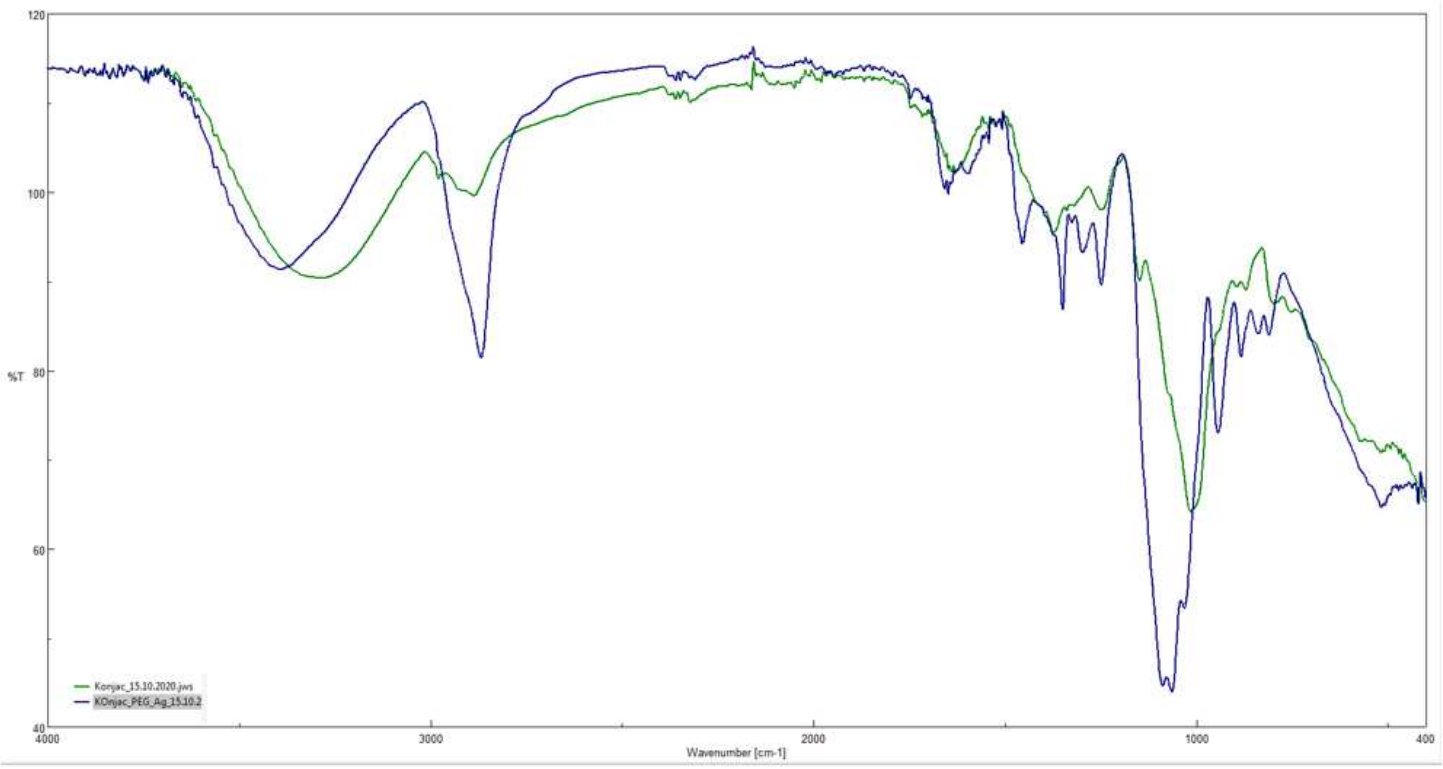

Figure 3

FTIR analysis of (a) pure KG and (b) KG/PEG-Ag NPs

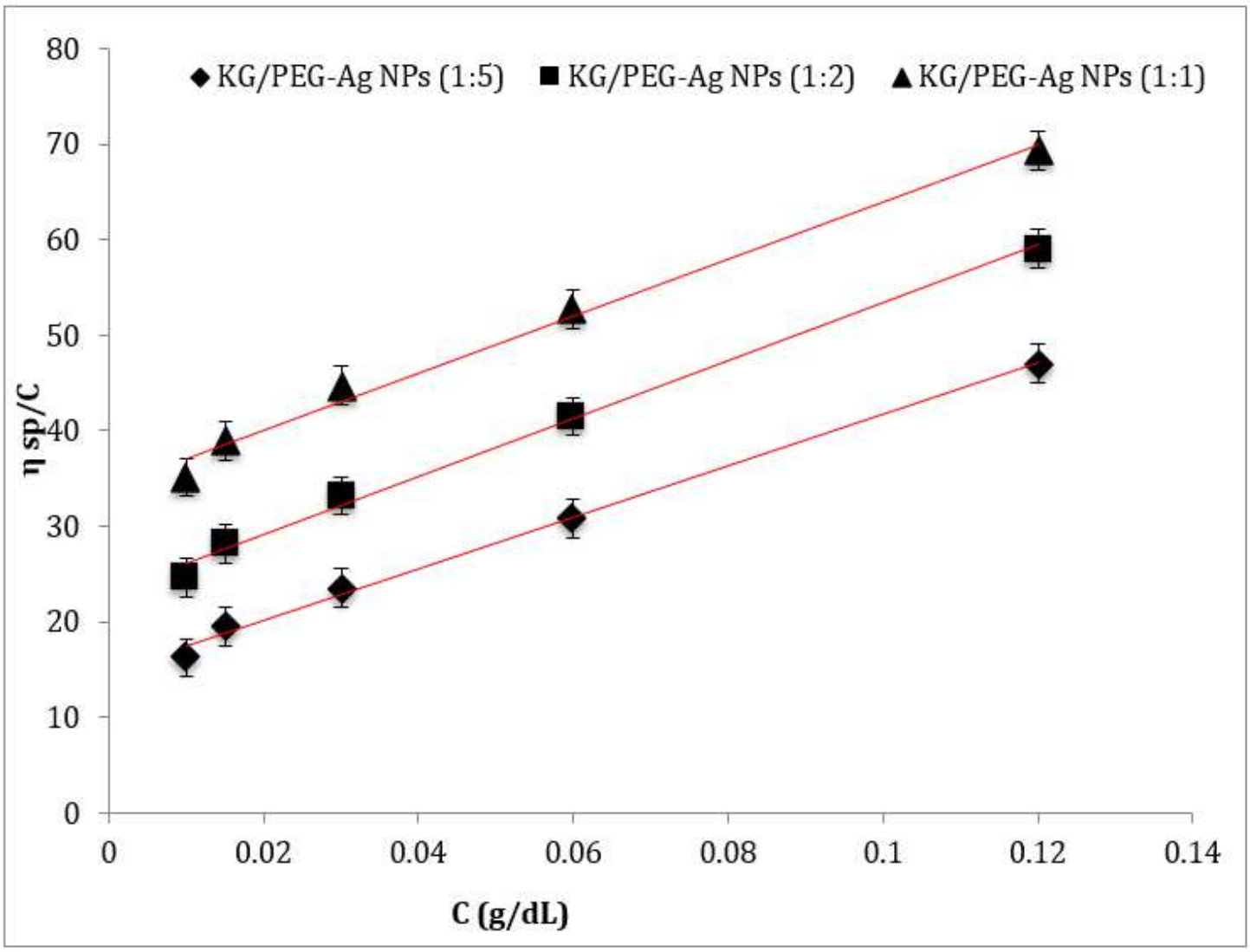

Figure 4

The effect of the blend of ratios of KG/PEG (wt./wt.) (1:1, 1:2, and 1:5) on [η] of the amplitude sonication 45%, sonication time 10 min, and temperature 25).

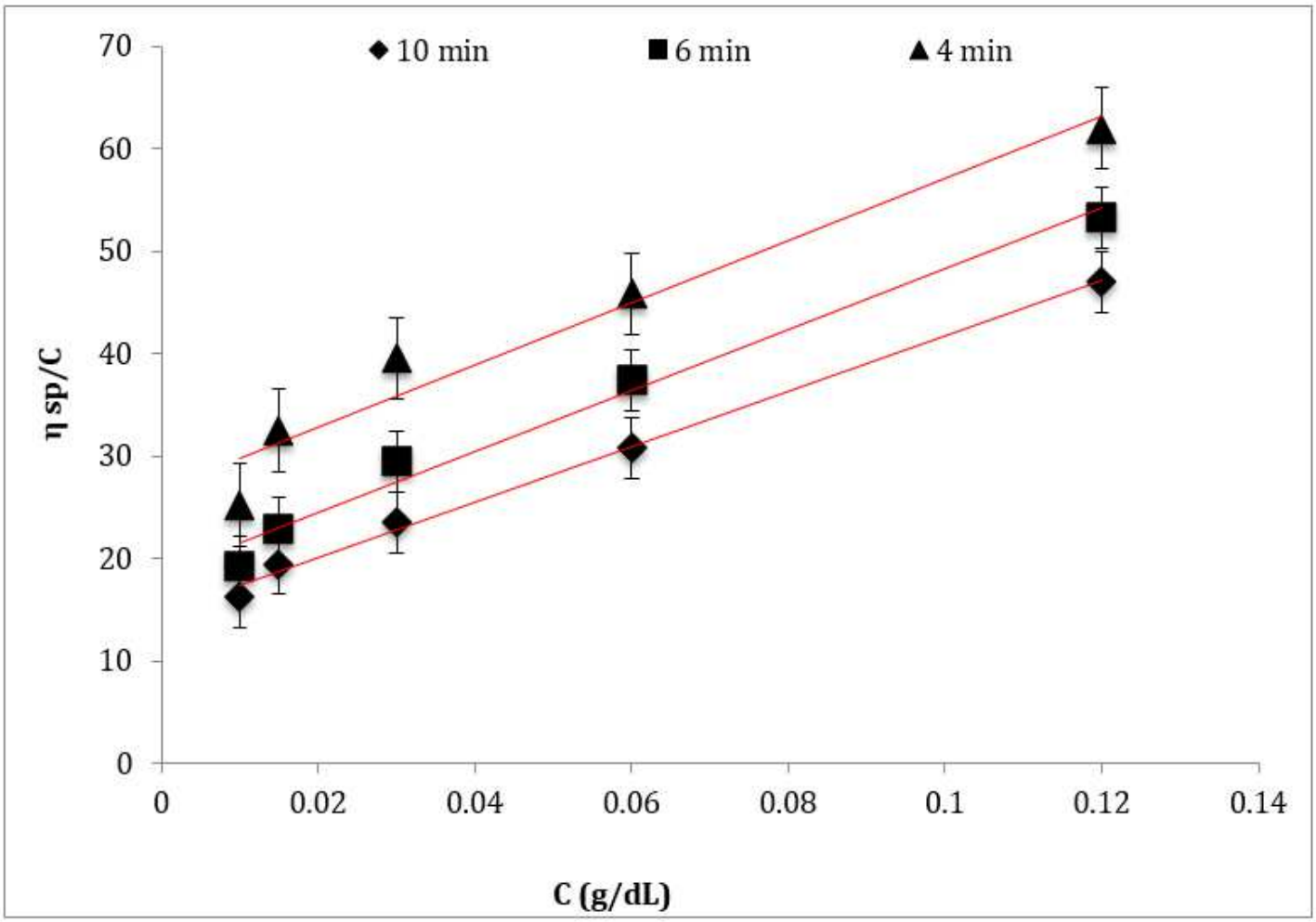

Figure 5

The effect of the sonication time (4-10 min) on [η] of KG/PEG-Ag NPs (ratio 1:5, the amplitude sonication 45%, and temperature 25)

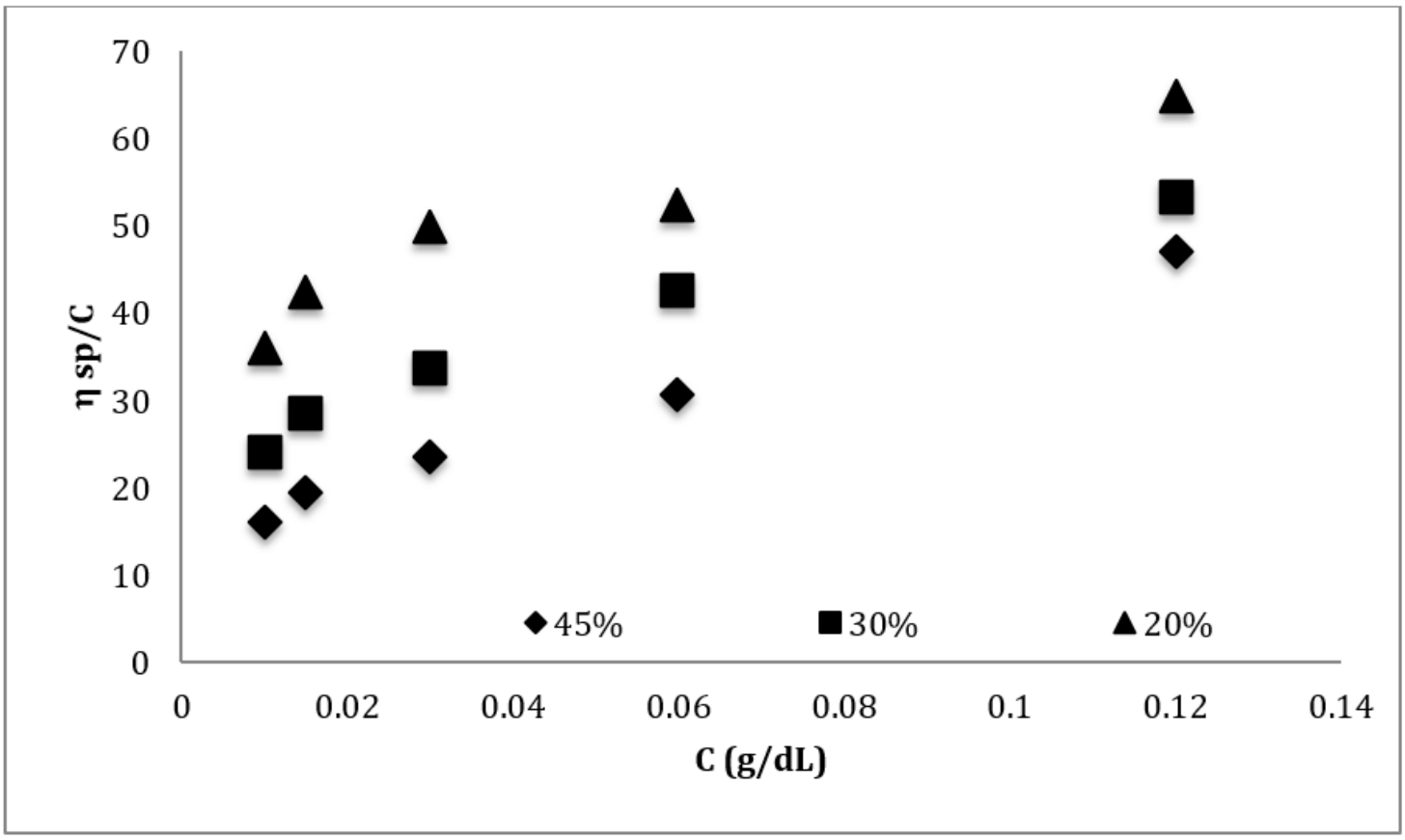

Figure 6

The effect of the amplitude of the sonication (20-45%) on [η] of KG/PEG-Ag NPs (the ratio of KG/PEG 1:5, sonication time 10 min, and temperature 25)

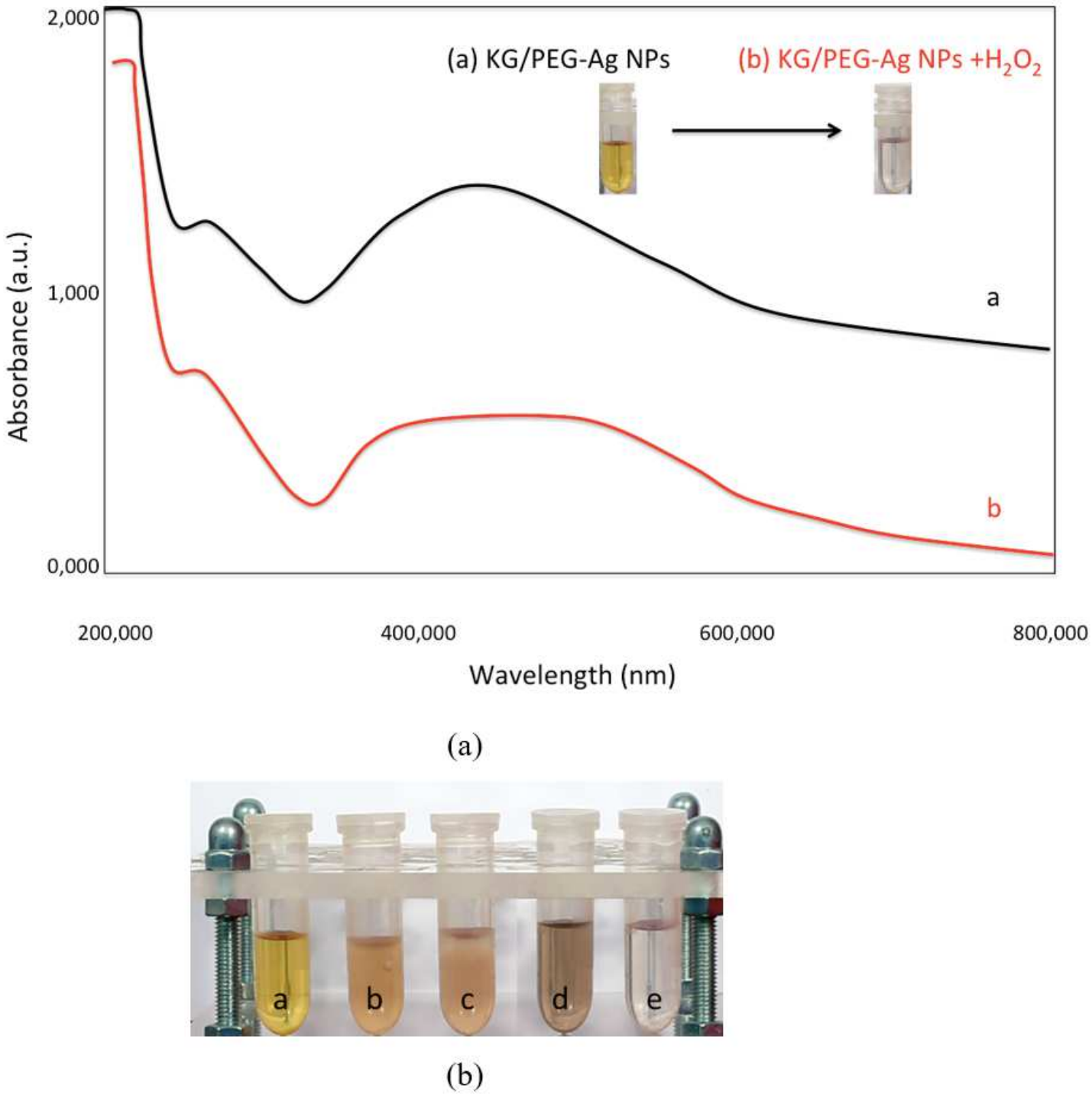

Figure 7

(A) UV-vis absorption spectra of KG/PEG-Ag NPs and KG/PEG-Ag NPs + H2O2, (B) Photographs of the selective colorimetric measurements of KG/PEG-Ag NPs (1:5) with different analytes such as (a) KG/PEG-Ag NPs in the absence of analyte, (b) in the presence of Omega 3, (c) testosterone, (d) progesterone, and (e) hydrogen peroxide

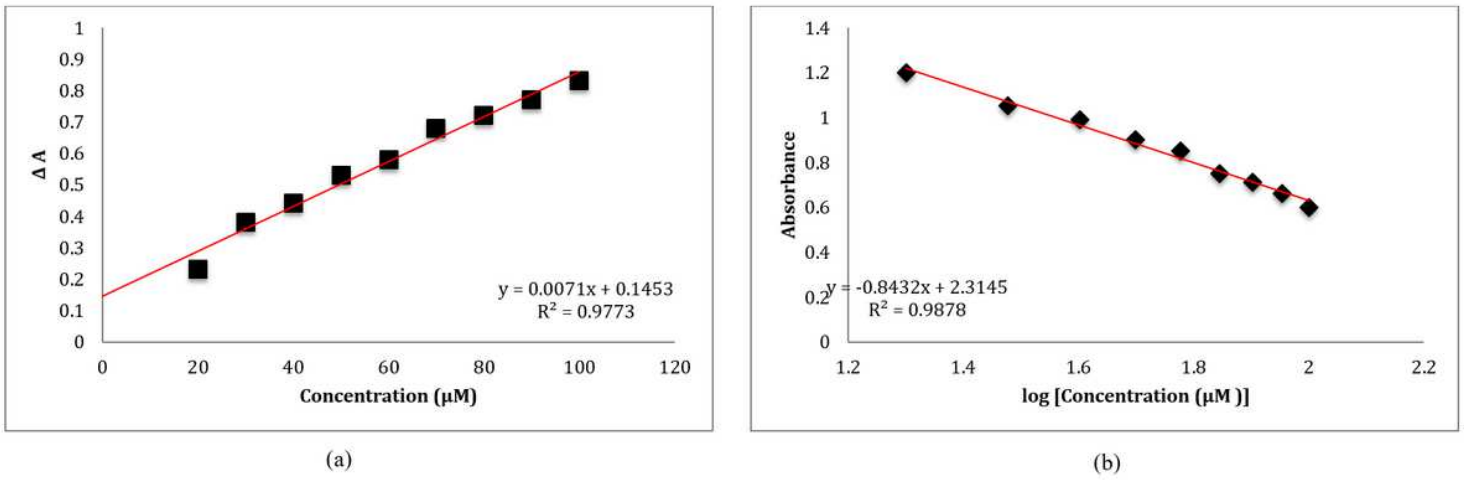

(a) (b)

Figure 8

The linear calibration plots of (a) the absorption intensity (ΔA), and (b) the absorbance of the KG/PEG-Ag NPs by varying the concentrations of H2O2 (1 -100 μM)

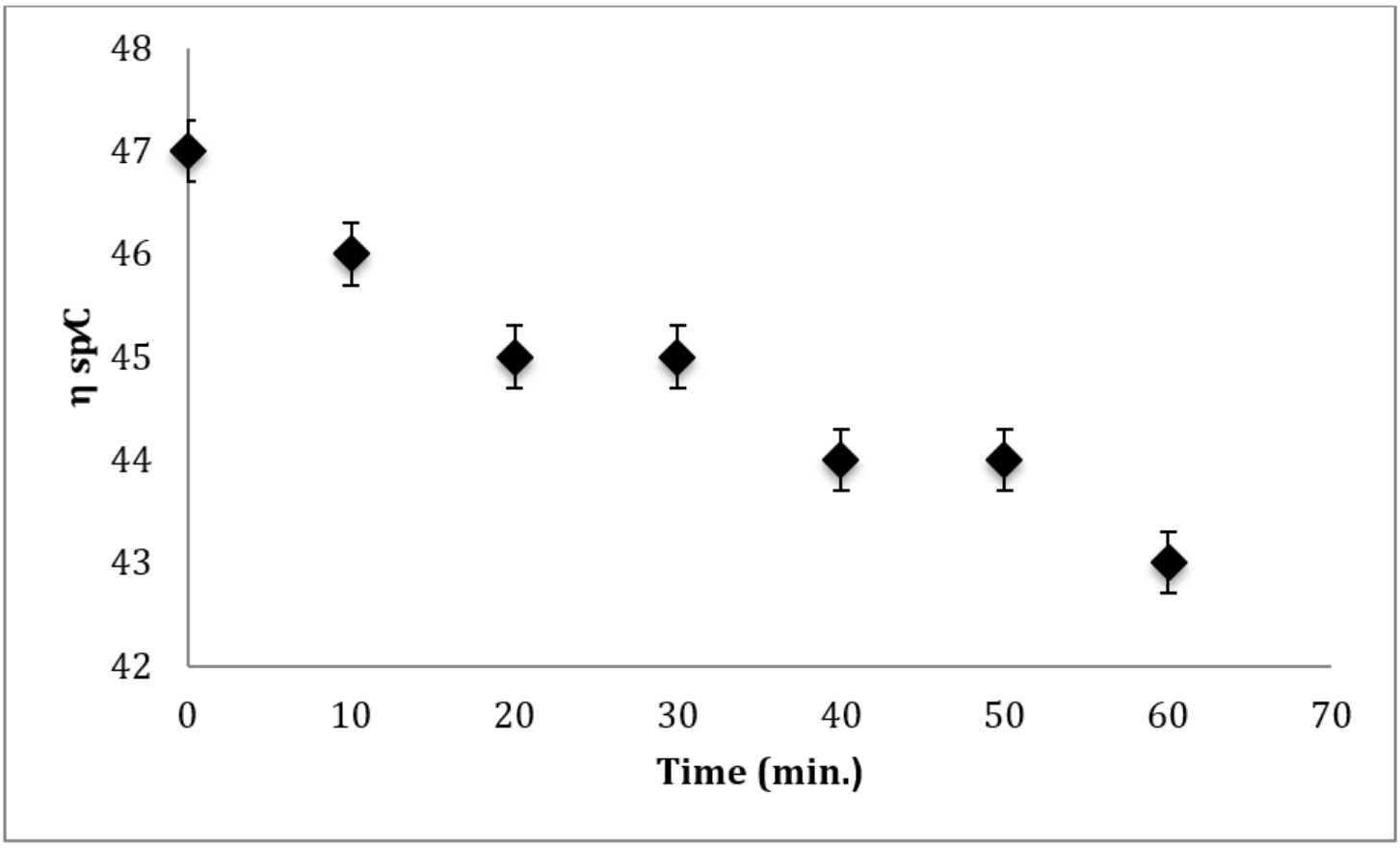

Figure 9

The effect of the ultraviolet factor on KG/PEG-Ag NPs (1:5) on [η]